

# Application of Phase Correlation to the Montage Synthesis and Three-Dimensional Reconstruction of Large Tissue Volumes from Confocal Laser Scanning Microscopy

Mohamed-Adel Slamani,<sup>1</sup> Andrzej Krol,<sup>2,\*</sup> Jacques Beaumont,<sup>3</sup> Robert L. Price,<sup>4</sup> Ioana L. Coman,<sup>5</sup> and Edward D. Lipson<sup>6</sup>

<sup>1</sup>ITT Industries, Advanced Engineering and Sciences, Alexandria, VA 22315, USA

<sup>2</sup>Department of Radiology, State University of New York Upstate Medical University, 750 E. Adams St., Syracuse, NY 13210, USA

<sup>3</sup>Department of Pharmacology, State University of New York Upstate Medical University, 750 E. Adams St., Syracuse, NY 13210, USA

<sup>4</sup>Department of Developmental Biology and Anatomy, School of Medicine, University of South Carolina, 6439 Garners Ferry Road, Columbia, SC 29209, USA

<sup>5</sup>Department of Mathematics and Computer Science, Ithaca College, 401C Williams Hall, Ithaca, NY 14850, USA

<sup>6</sup>Department of Physics, Syracuse University, Syracuse, NY 13244-1130, USA

**Abstract:** We have implemented and tested a new automatic method for the montage synthesis and three-dimensional (3D) reconstruction of large tissue volumes from confocal laser scanning microscopy data (CLSM). This method relies on maximization of the phase correlation between adjacent images. It was tested on a large specimen (a murine heart) that was cut into a number of individual sections with thickness appropriate for CLSM. The sections were scanned horizontally (in-plane) and vertically (perpendicular to the optical planes) to produce “tiles” of a 3D volume. Phase correlation maximization was applied to the montage synthesis of in-plane tiles and 3D alignment of optical slices within a given physical section. The performance of the new method is evaluated.

**Key words:** montage synthesis, image mosaicking, phase correlation, confocal laser scanning microscopy

## INTRODUCTION

The ability to analyze the organization of a relatively large (i.e., tens of millimeters) biological sample in three dimensions is becoming increasingly critical in biomedical research (Brakenhoff et al., 1985; Carlsson et al., 1985; Boon et al., 1994; Merchant et al., 1994; Prakash et al., 1994; O'Brien et al., 2000; Liu & Chiang, 2003). Very high spatial resolution (submicrometer) can be obtained from confocal laser scanning microscopy (CLSM) (Davidotts & Egger, 1969; Denk et al., 1990). However, because of light absorption and scatter, typically only 100–200- $\mu\text{m}$ -thick physical sections can be imaged at a time at low magnifications and much less than this at higher magnifications. This necessitates cutting a large specimen into a number of individual sections with appropriate thickness. Each physical slice can then be imaged by recording a series (i.e., a stack) of images

in parallel optical planes, defined by varying the axial focal depth. Imaging of structure with a large transaxial cross section requires a number of individual, in-plane images, referred to as “tiles,” which form pieces of a “mosaic.” The tiles have to be montaged or mosaicked together to form a single integrated transaxial image in a given optical plane. This process is referred to as “mosaicking.” Building a three-dimensional (3D) image from 2D tiles obtained for a number of individual physical sections requires three steps: (1) 2D registration of tiles, (2) 3D alignment of reconstructed optical slices within a given physical section, and (3) 3D alignment of reconstructed physical sections.

There exist a number of approaches to 2D montage synthesis (mosaicking) within a given optical plane. They can be separated into two groups: the first group involves man in the loop and consists of manual fitting of the overlapping tiles (Oldmixon & Carlsson, 1993; Beck et al., 2000) and the second group involves automated methods that do not require a man-in-the-loop setting. The automated methods rely on optimization of some similarity measure between the overlapping parts of the images, includ-

ing the sum of absolute valued differences, the normalized correlation coefficient, the mutual information function (Fraser & Swinney, 1986), a landmark-based method (Becker et al., 1996), and a model-based minimum mean squared algorithm (Can et al., 2003). The 2D montage synthesis within a given optical plane yields an optical slice. Optical slices can be aligned with respect to each other to form a 3D object—a single CLSM section. The 3D alignment of the optical slices has been performed through either manual or automated alignment of segmented contours in each optical plane (Oldmixon & Carlsson, 1993) or through application of a suitable registration algorithm to all the optical planes forming the entire CLSM data set (Roysam et al., 1994; Capek & Krekule, 1999) or based on high-order transformation models (Al-Kofahi et al., 2003). Once a single CLSM section is obtained, its surface can be extracted using various methods (Hessler et al., 1992).

Baheerathan et al. (1998) reported on a semiautomatic interactive registration method for 3D reconstruction of successive serial transmission electron micrographs of ultrathin sections of mouse liver cell nuclei. The phase correlation method was used to correct the rotation and translation components followed by the global distortion correction via a point mapping method based on different ways of selecting the control points.

In this article we describe the application of an image-processing procedure, based on the phase-correlation method, to enable the fully automated 2D registration of in-plane images (i.e., tiles), and 3D alignment of reconstructed (montaged) optical slices within a given physical section. The procedure has been tested on the whole set of CLSM images of a murine heart. The size of the 3D reconstruction space containing all the montaged optical slices and all the assembled in 3D CLSM sections forming the imaged specimen was approximately  $10 \text{ mm} \times 10 \text{ mm} \times 10 \text{ mm}$ .

## MATERIALS AND METHODS

### Sample Preparation and Image Acquisition

Murine hearts were immersion fixed for 24 h in 4% paraformaldehyde and were sectioned (100–150  $\mu\text{m}$ ) on an Oxford vibratome. Sections were rinsed in PBS containing 0.1 M glycine and 1% BSA and stained with a 1:20 dilution (10 units/slide) of rhodamine phalloidin (Molecular Probes, Eugene, OR) in PBS overnight at 4°C. Rhodamine phalloidin is a specific stain for *f*-actin, which is a primary component of the cardiac contractile apparatus. Imaging was performed with a  $4\times$  (NA 0.2/WD 15.7) objective on a BioRad MRC1024 ES confocal microscope equipped with an argon/krypton laser. Each image consisted of a  $512 \times 512$  pixel array and each pixel was  $4.83 \mu\text{m}^2$ . Each optical Z-series through the vibratome sections was collected at 5- $\mu\text{m}$  intervals and, for each vibratome section, it was

necessary to collect images from several overlapping areas to complete a montaged image of the entire heart. Data sets were converted from the BioRad pic format to standard uncompressed tiff images in order to be analyzed.

### Mosaicking In-Plane Tiles into an Optical Slice

Denote by  $XY$  an in-plane coordinate system. Because the microscope stage moves only horizontally in the  $X$  and  $Y$  directions and does not perform any rotations, the relationship between overlapping tiles consists of a straight-line shift in the  $XY$  direction. As a result, an image-processing procedure derived from phase correlation can be designed for the mosaicking task. The *phase correlation* approach is based on frequency analysis of data correlation between two in-plane images and stems from the property that translation in the space domain corresponds to a phase shift in the frequency domain (Kuglin & Hines, 1975; Bracewell et al., 1993; Foroosh et al., 2002)

Taking the inverse Fourier transform (IFT) of the phase shift and then finding the maximum amplitude yields the  $XY$  displacement. Whenever the two images are identical in content and related by pure in-plane translation  $(X_0, Y_0)$ , IFT results in a delta function centered around the displacement  $(X_0, Y_0)$ .

Let  $f_1(x, y)$  and  $f_2(x, y)$  denote functions of pixel values in images 1 and 2, respectively (Foroosh et al., 2002). Further, let

$$f_2(x, y) = f_1(x - x_0, y - y_0) \quad (1)$$

According to the Fourier shift property,

$$F_2(u, v) = F_1(u, v)e^{-j(ux_0 + vy_0)}, \quad (2)$$

where  $F_m(u, v)$  denote the Fourier transform of  $f_m(x, y)$ ,  $m = 1, 2$ . The normalized cross power spectrum is given by

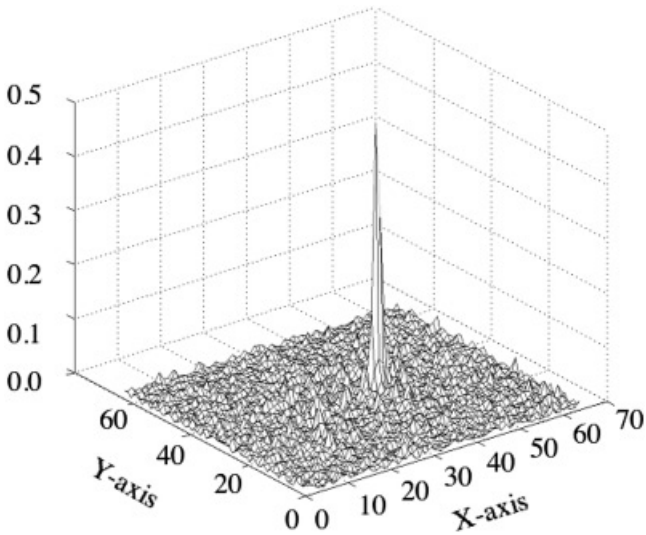
$$\frac{F_2(u, v)F_1^*(u, v)}{|F_2(u, v)F_1^*(u, v)|} = e^{-j(ux_0 + vy_0)}, \quad (3)$$

where  $*$  denotes the complex conjugate. Taking the IFT of the normalized cross power spectrum in (3) results in a Dirac delta function centered at  $(x_0, y_0)$ :

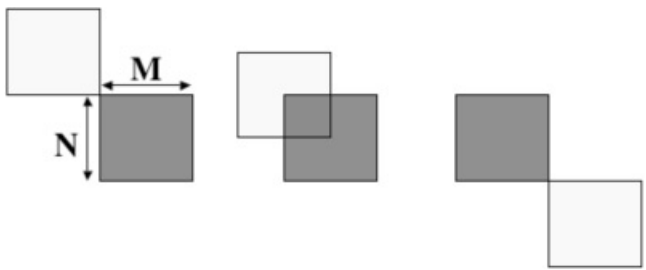
$$e^{-j(ux_0 + vy_0)} \rightarrow \delta(x - x_0, y - y_0). \quad (4)$$

Figure 1 illustrates results of operations defined by equations (1)–(4) performed on two adjacent CLSM images (tiles) located in the same optical plane and having large overlap.

In the case of confocal image tiles, the difference between the two images is not a simple shift (i.e., translation) but involves disjoint areas that cannot be found in both images at once. Some structures disappear from the image



**Figure 1.** The amplitude of the 2D inverse Fourier transform performed on the normalized cross power spectrum of two adjacent CLSM images (tiles) located in the same optical plane ( $XY$ ), having large overlap and related by pure in-plane translation defined by the vector  $(X_0, Y_0) = (40, 30)$ ; see equations (1)–(4) in the text. Note the sharp peak, representing the Dirac delta function, centered at  $(X_0, Y_0)$ .



**Figure 2.** Possible pixel shifts between consecutive  $M \times N$  tiles. Left:  $x_0 = 0$  and  $y_0 = 0$ ; center:  $x_0 = M/2$  and  $y_0 = N/2$ ; right:  $x_0 = 2M$  and  $y_0 = 2N$ .

and other structures emerge when going from one tile to the other. This causes the appearance of the high-intensity side lobes while broadening and reducing the delta-function peak, thus making it difficult to find the location of the actual peak. Another major problem is that although the size of a tile and its FFT is limited to  $M \times N$ , the shift in phase can be up to  $2M \times 2N$  because of the extent by which one tile can move relative to another, as shown in the examples of Figure 2. Because of the  $M \times N$  limitation, a higher phase indication is “wrapped” into the smaller values, making it difficult to decide whether the value obtained for a shift is real or wrapped. These factors have been successfully addressed in the present work.

The algorithms for montage synthesis via phase correlation (MSPC2D) in 2D (i.e., for mosaicking of CLSM

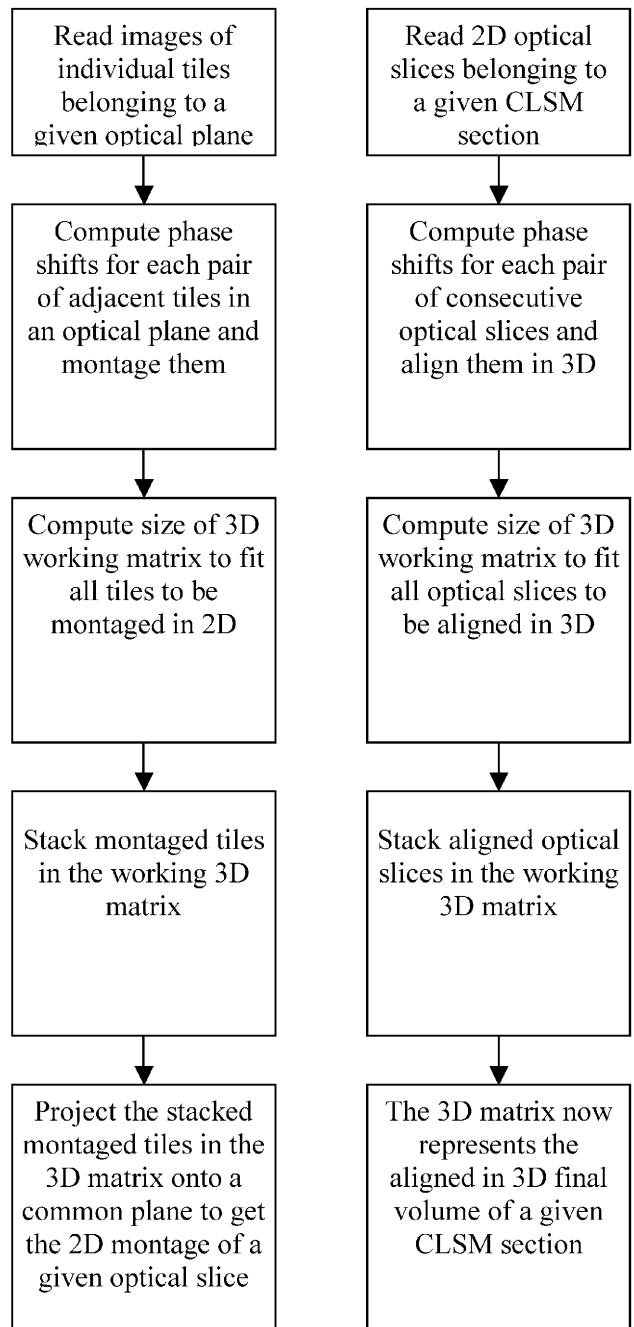


**Figure 3.** Flowchart of the phase correlation algorithms. Left: MSPC2D algorithm used to montage the individual LSCM two-dimensional images (tiles) belonging to the same optical plane; right: MSPC3D algorithm used to align the synthesized optical slices to form the 3D volume of a given physical section.

optical slices) and for 3D alignment of optical slices via phase correlation (MSPC3D) were coded in MATLAB (The MathWorks, Inc., Natick, MA). The MSPC2D algorithm was applied to each pair of adjacent tiles in each CLSM optical plane, and then, using one tile as a reference, an optical slice was built by montage (mosaicking) all the tiles belonging

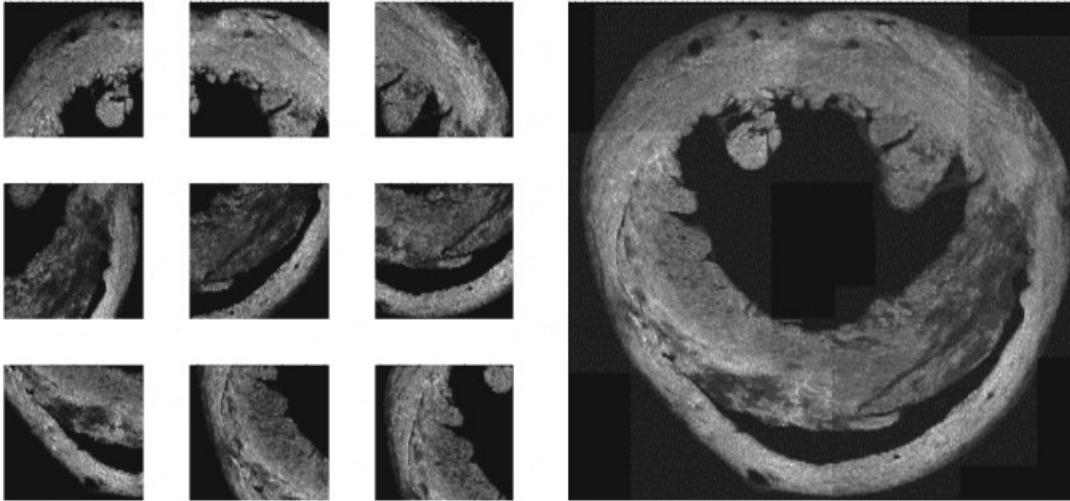


**Figure 4.** Example of montage synthesis (mosaicking). Left:  $512 \times 512$  pixel tiles; right: the resulting montage (mosaic) of up to  $1536 \times 1536$  pixels. Pixel size is  $4.83 \mu\text{m} \times 4.83 \mu\text{m}$ .

to that optical plane. The approach was tested on all the data and proved to be 99% successful. The flowchart of the MSPC2D algorithm is shown in Figure 3. The algorithm utilizes a 3D matrix as a working space where the montaged adjacent tiles are stored. Once all the tiles are montaged with their neighbors, the final image of an optical slice is obtained by projecting (properly normalized) all the montaged images onto a common plane. The MSPC3D algorithm was subsequently applied to all already montaged optical slices belonging to a given CLSM section, yielding a synthesized 3D object correctly mapping the selected vibratome section of the murine heart. The approach was tested on all the data and proved to be 100% successful. The flowchart of the MSPC3D algorithm is shown in Figure 3. It also utilizes a 3D matrix as a working space where the aligned consecutive optical slices are stored.

## RESULTS

Our test CLSM data set obtained for a murine heart consisted of 10,800 images (i.e., individual tiles) each of size  $512 \times 512$  pixels (pixel size  $4.83 \mu\text{m}$ , 262 kB), forming a set of data with total size of 2.8 GB. The set contains 72 physical (vibratome) sections, each  $150 \mu\text{m}$  thick. Each vibratome section was divided into approximately 30 parallel optical planes (Z-series)  $5 \mu\text{m}$  apart. A 1.5-GHz computer with 1 GB of RAM was used to process all tiles in all optical planes. A total of 1,459 mosaic images (optical slices) were constructed. The total time elapsed was (a) 22 h to build individual-optical-plane images (2D mosaicking using MSPC2D algorithm), and (b) 28 h to align all individual-optical-plane images within each vibratome section (3D alignment using MSPC3D algorithm).

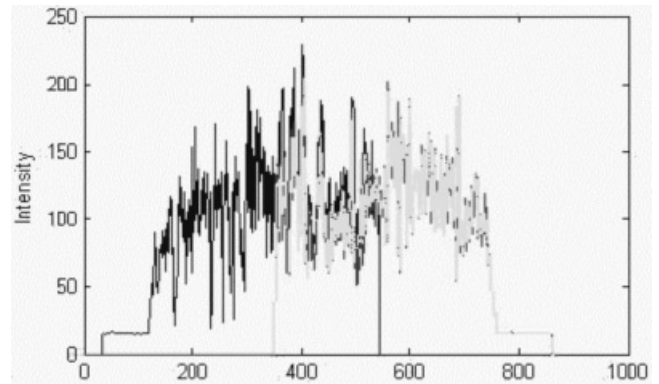


**Figure 5.** Line profiles showing intensity values for row 200 versus pixel number in the montaged tiles 1 (black line) and 2 (gray line). The data are obtained from row 200 of the two top left tiles of Figure 4.

### Montage Synthesis of Individual Image Tiles within an Optical Plane

Figure 4 shows an example of adjacent image tiles and the resulting mosaic obtained using MSPC2D algorithm. The quality of 2D image integration can be evaluated by inspecting line profiles through the images (Fig. 5). Very similar bias, noise, and signal levels are evident in both profiles. The only cases for which the phase correlation method failed were those that had very small or no overlapping regions between two consecutive tiles (Fig. 6a). Even in those cases, however, the procedure worked successfully, just by rearranging the order of the consecutive tiles and choosing a different reference tile. The corrected version of Figure 6a is shown in Figure 6b.

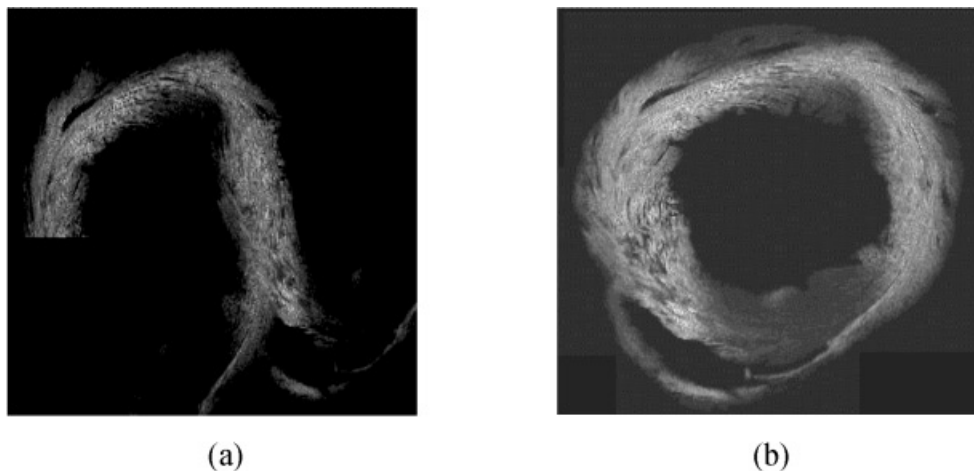


**Figure 6.** Performance of phase-correlation algorithm for in-plane montage synthesis. **a:** incorrectly synthesized montage attributable to insufficient or nonoverlapping regions between adjacent tiles; **b:** correctly synthesized montage of the same set of tiles as in **a** obtained after rearranging the order of tiles in the phase-correlation procedure. Image size is  $1536 \times 1536$  pixels. Pixel size is  $4.83 \mu\text{m} \times 4.83 \mu\text{m}$ .

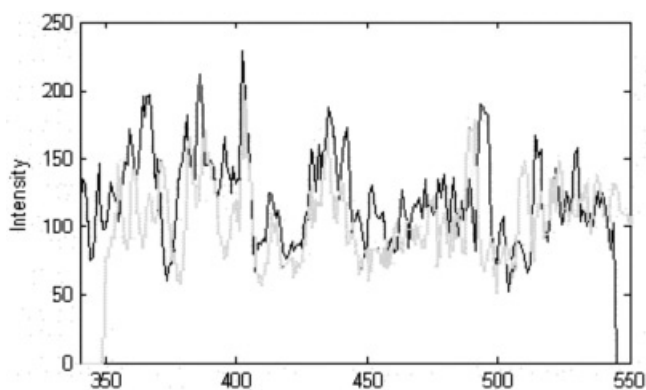


**Figure 7.** Example of the line profiles showing intensity values versus pixel number in two neighboring tiles, black and gray, respectively, that were aligned using the phase-correlation method. Small local misalignment is due to noise in the images.

Because of noise in the images, the centroids of the local minima and maxima could be aligned only on average, resulting in possible small local misalignment (Fig. 7). However, we estimate that the resolution loss attributable to this phenomenon is below 2 pixels.

Contrast variation among tiles corresponding to the same optical plane has not created any problems in the phase-correlation mosaicking procedure (Fig. 8).

### Alignment of Individual Optical Slices within a Physical Section

Consecutive optical slices within a given physical section are acquired via vertical translation of the sample stage. Again, because no rotations are involved, this 3D alignment can be

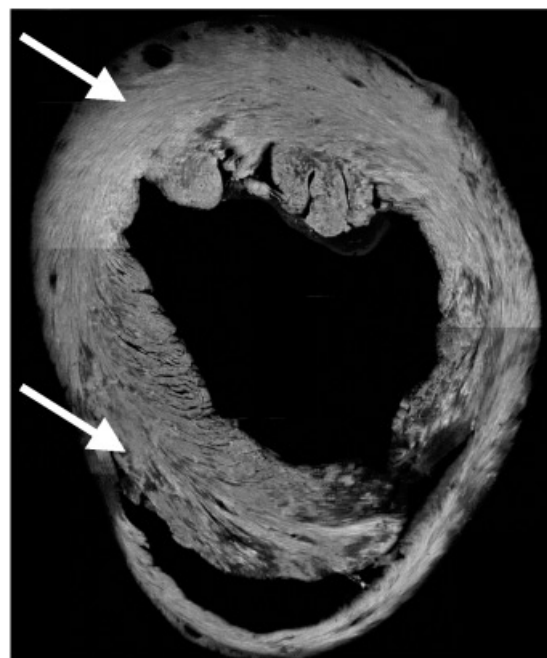


**Figure 8.** Optical plane successfully synthesized via the phase-correlation method containing tiles exhibiting intensity variation (arrows). Image size is  $1536 \times 1536$  pixels. Pixel size is  $4.83 \mu\text{m} \times 4.83 \mu\text{m}$ .

achieved by finding the straight  $xy$  phase shift between consecutive optical slices. The above-described MSPC3D algorithm, utilizing phase correlation, was used for this task with complete success. Figure 9 shows an alignment of two consecutive optical slices. Figure 10 shows a complete reconstructed volume of one vibratome section.

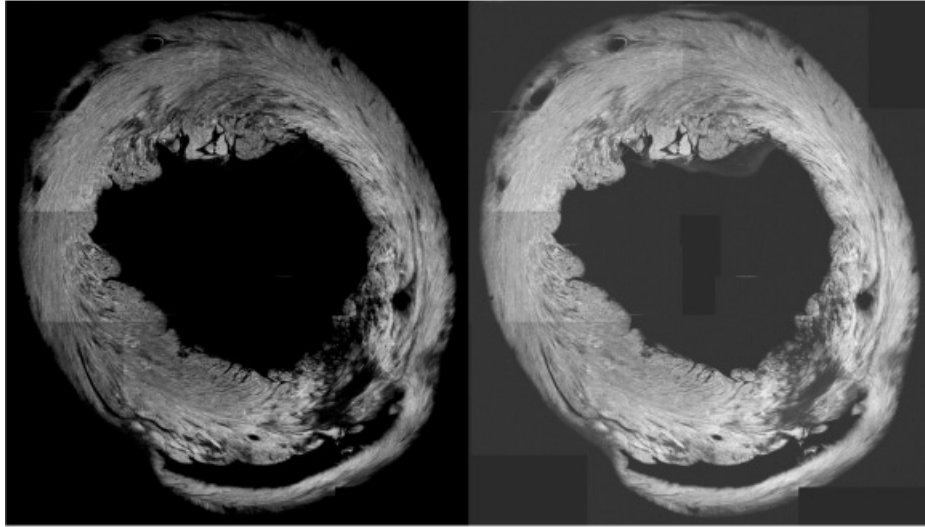


**Figure 9.** Example of two consecutive optical planes belonging to the same physical section aligned using the phase-correlation procedure. Image size is  $1536 \times 1536$  pixels. Pixel size is  $4.83 \mu\text{m} \times 4.83 \mu\text{m}$ .

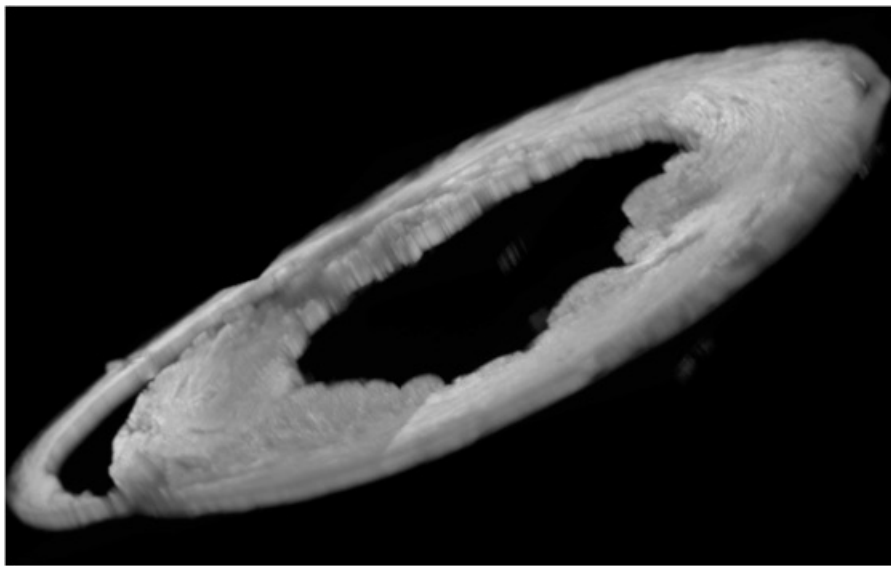


**Figure 10.** Example of a physical section (section 28) that comprises 30 optical slices (each of them synthesized via the phase-correlation method) aligned in three dimensions using the phase-correlation procedure. Image size is  $1536 \times 1536 \times 30$  voxels. Voxel size is  $4.83 \mu\text{m} \times 4.83 \mu\text{m} \times 5 \mu\text{m}$ .

## CONCLUSIONS

The reported study was performed on only one sample—a murine heart sectioned using vibratome and imaged with CLSM. However, we believe that the conclusions are general and can be extended to any sample imaged with laser scanning microscopy (LSM) including multiphoton laser scanning microscopy (MLSM) independent of the sectioning and staining method. Presently, we are performing sim-

ilar studies on another murine heart that was vibratome sectioned and imaged with  $10\times$  magnification using CSLM with three different stains resulting in three different colors (red, green, and blue). The resulting imaged volume in terms of a total number of voxels will be significantly larger and it will be interesting to assess how our algorithms perform in this context. We plan to publish the results as soon as possible.

The phase-correlation procedure (MSPC2D algorithm) was 99% successful in 2D montage synthesis. The only cases

for which the method failed involved those involving optical slices that had very small or no overlapping regions between consecutive image tiles (Fig. 6a). However, even in those cases, the procedure worked successfully after rearranging the order of the tiles (Fig. 6b). The 3D synthesis using phase correlation (MSPC3D algorithm) was 100% successful in alignment of optical slices within a given physical section (Fig. 10).

The phase-correlation-based procedure offers a very efficient and robust approach to building a large 3D volume from 2D image tiles obtained by CLSM in a series of optical planes in the same vibratome section of the sample. A proper preparation of the samples would require implementation of a CLSM or MLSM software that would (a) perform error checking to detect inadequate overlap between consecutive tiles, and (b) check whether all tiles in all optical planes have been acquired. In cases where there are such problems, rescanning would then be done automatically. As a result, the 1% failure rate in 2D mosaicking would be remedied.

The same algorithms without any modifications can be used for the montage synthesis of 2D optical slices and the 3D tissue reconstruction of large tissue volumes in MLSM with the added advantage of deeper sectioning available in MLSM.

We plan to implement our algorithms in the ITK framework ([www.itk.org](http://www.itk.org)) and make them available to the LSM community.

More work and a different approach are required to implement 3D registration of consecutive physical sections, because the process of sectioning is done mechanically and results in loss of material ( $\sim 5 \mu\text{m}$  thick), inadvertent relative rotation, tilt, and distortion of consecutive physical sections.

## ACKNOWLEDGMENTS

This work was partially supported by an internal grant from the Department of Radiology, SUNY Upstate Medical University.

## REFERENCES

- AL-KOFAHI, O., CAN, A., LASEK, S., SZAROWSKI, D.H., TURNER, J.N. & ROYSAM, B. (2003). Algorithms for accurate 3D registration of neuronal images acquired by confocal scanning laser microscopy. *J Microsc* **211**, 8–18.
- BAHEERATHAN, S., ALBREGTSEN, F. & DANIELSEN, H.E. (1998). Registration of serial sections of mouse liver cell nuclei. *J Microsc* **192** (Pt 1), 37–53.
- BECK, J.C., MURRAY, J.A., WILLOWS, A.O. & COOPER, M.S. (2000). Computer-assisted visualizations of neural networks: Expanding the field of view using seamless confocal montage. *J Neurosci Methods* **98**, 155–163.
- BECKER, D.E., ANCIN, H., SZAROWSKI, D.H., TURNER, J.N. & ROYSAM, B. (1996). Automated 3-D montage synthesis from laser-scanning confocal images: Application to quantitative tissue-level cytological analysis. *Cytometry* **25**, 235–245.
- BOON, M.E., SCHUT, J.J., BENITA, E.M. & KOK, L.P. (1994). Confocal optical sectioning and three-dimensional reconstruction of carcinoma fragments in Pap smears using sophisticated image data processing. *Diagn Cytopathol* **10**, 268–275.
- BRACEWELL, R.N., CHANG, K.-Y., JHA, A.K. & WANG, Y.-H. (1993). Affine theorem for two-dimensional Fourier transform. *Electron Lett* **29**, 304–306.
- BRAKENHOFF, G.J., VAN DER VOORT, H.T., VAN SPRONSEN, E.A., LINNEMANS, W.A. & NANNINGA, N. (1985). Three-dimensional chromatin distribution in neuroblastoma nuclei shown by confocal scanning laser microscopy. *Nature* **317**, 748–749.
- CAN, A., AL-KOFAHI, O., LASEK, S., SZAROWSKI, D.H., TURNER, J.N. & ROYSAM, B. (2003). Attenuation correction in confocal laser microscopes: A novel two-view approach. *J Microsc* **211**, 67–79.
- CAPEK, M. & KREKULE, I. (1999). Alignment of adjacent picture frames captured by a CLSM. *IEEE Trans Inf Technol Biomed* **3**, 119–124.
- CARLSSON, K., DANIELSSON, P., LENZ, R., LILJEBORG, A., MAJLOF, L. & ÅSLUND, N. (1985). Three-dimensional microscopy using a confocal laser scanning microscope. *Optics Lett* **10**, 53–55.
- DAVIDOTTS, P. & EGGER, M.D. (1969). Scanning laser microscopy. *Nature* **233**, 831–835.
- DENK, W., STRICKLER, J.H. & WEBB, W.W. (1990). Two-photon laser scanning fluorescence microscopy. *Science* **248**, 73–76.
- FOROOSH, H., ZERUBIA, J.B. & BERTHOD, M. (2002). Extension of phase correlation to subpixel registration. *Proc IEEE Trans Image Process* **11**, 188–200.
- FRASER, A.M. & SWINNEY, H.L. (1986). Independent coordinates for strange attractor from mutual information. *Phys Rev A* **33**, 1134–1140.
- HESSLER, D., YOUNG, S.J., CARRAGHER, B.O., MARTONE, M.E., LAMONT, S., WHITTAKER, M., MILLIGAN, R.A., MASLIAH, E., HINSHAW, J.E. & ELLISMAN, M.H. (1992). Programs for visualization in three-dimensional microscopy. *Neuroimage* **1**, 55–67.
- KUGLIN, C. & HINES, D. (1975). The phase correlation image alignment method. In *Proceedings of the IEEE International Conference on Cybernetics and Society*, Vol. 7, pp. 163–165. New York: Institute of Electrical and Electronics Engineers.
- LIU, Y.C. & CHIANG, A.S. (2003). High-resolution confocal imaging and three-dimensional rendering. *Methods* **30**, 86–93.
- MERCHANT, F.A., AGGARWAL, S.J., DILLER, K.R. & BOVIK, A.C. (1994). In-vivo analysis of angiogenesis and revascularization of transplanted pancreatic islets using confocal microscopy. *J Microsc* **176** (Pt 3), 262–275.
- O'BRIEN, F.J., TAYLOR, D., DICKSON, G.R. & LEE, T.C. (2000). Visualisation of three-dimensional microcracks in compact bone. *J Anat* **197** (Pt 3), 413–420.
- OLDMIXON, E.H. & CARLSSON, K. (1993). Methods for large data volumes from confocal scanning laser microscopy of lung. *J Microsc* **170** (Pt 3), 221–228.
- PRAKASH, Y.S., SMITHSON, K.G. & SIECK, G.C. (1994). Application of the Cavalieri principle in volume estimation using laser confocal microscopy. *Neuroimage* **1**, 325–333.
- ROYSAM, B., ANCIN, H., BHATTACHARJYA, A.K., CHISTI, M.A., SEEGAL, R. & TURNER, J.N. (1994). Algorithms for automated characterization of cell populations in thick specimens from 3-D confocal fluorescence microscopy data. *J Microsc* **173** (Pt 2), 115–126.